MOLECULAR AND CELLULAR BIOLOGY, Jan. 2010, p. 54–67 Vol. 30, No. 1
0270-7306/10/$12.00 doi:10.1128/MCB.00248-09

Fluorescence Resonance Energy Transfer Analysis of Merlin Conformational Changes▽

Robert F. Hennigan,[1]† Lauren A. Foster,[1] Mary F. Chaiken,[1] Timmy Mani,[1] Michelle M. Gomes,[2] Andrew B. Herr,[2] and Wallace Ip[1]*

Departments of Cancer & Cell Biology[1] and Molecular Genetics, Biochemistry & Microbiology,[2] University of Cincinnati, College of Medicine, Cincinnati, Ohio 45267

Received 25 February 2009/Returned for modification 30 March 2009/Accepted 15 October 2009

Neurofibromatosis type 2 is an inherited autosomal disorder caused by biallelic inactivation of the *NF2* tumor suppressor gene. The *NF2* gene encodes a 70-kDa protein, merlin, which is a member of the ezrin-radixin-moesin (ERM) family. ERM proteins are believed to be regulated by a transition between a closed conformation, formed by binding of their N-terminal FERM domain and C-terminal tail domain (CTD), and an open conformation, in which the two domains do not interact. Previous work suggests that the tumor suppressor function of merlin is similarly regulated and that only the closed form is active. Therefore, understanding the mechanisms that control its conformation is crucial. We have developed a series of probes that measures merlin conformation by fluorescence resonance energy transfer, both as purified protein and in live cells. Using these tools, we find that merlin exists predominately as a monomer in a stable, closed conformation that is mediated by the central α-helical domain. The contribution from the FERM-CTD interaction to the closed conformation appears to be less important. Upon phosphorylation or interaction with an effector protein, merlin undergoes a subtle conformational change, suggesting a novel mechanism that modulates the interaction between the FERM domain and the CTD.

Neurofibromatosis type 2 is an inherited autosomal disorder that is characterized by bilateral schwannomas of the eighth cranial nerve. The tumor suppressor gene responsible for this disorder, *NF2*, was cloned in 1993 (45). Biallelic inactivation of the *NF2* gene is also seen in spontaneous schwannoma, meningioma, and malignant mesothelioma (22). In mouse models, deletion of the *Nf2* gene is embryonic lethal, indicating an essential role for *NF2* in development (24). Heterozygous mice develop a variety of aggressive metastatic tumors that have lost the wild-type allele (23). Targeted deletion of the *Nf2* gene in Schwann cells leads to schwannoma formation (7). In vitro, *Nf2*-null cells grow to significantly higher densities (31), suggesting that contact inhibition of growth is impaired in these cells and that mediation of growth arrest at high cell density may be the basis for the tumor suppressor function of the *NF2* gene. In normal fibroblasts, merlin is inactive as a growth suppressor in subconfluent cells, becoming activated as they approach confluence, thereby effecting contact inhibition of growth (26).

The *NF2* gene encodes a 70-kDa protein called merlin (for moesin, ezrin, radixin-like protein), which shares significant homology with members of the ezrin-radixin-moesin (ERM) branch of the Band 4.1 superfamily (45). The domain structure of merlin, also shared with other ERM proteins, consists of an N-terminal FERM domain, followed by a central α-helical region (CH) and a C-terminal tail domain (CTD). The merlin FERM domain has relatively high sequence similarity with other ERM family members, a 60 to 70% identity over the first 300 amino acids. The CH domain and the CTD show much lower identity (28 to 36%); however, the α-helical character of the CH domain is preserved, as is the heptad repeat pattern typical of α-helices that form coiled coils (46).

The critical point of regulation of all the ERM proteins is a high-affinity intramolecular interaction between the C-terminal domain and the FERM domain (4) (Fig. 1). The FERM domain folds into a three-lobed cloverleaf structure that acts as a multifaceted docking site for protein binding partners (16, 39). The CTD, consisting of four major and two minor helices and a beta sheet, binds to the FERM domain by extending across the face of the F2 and F3 lobes (32). This intramolecular head-to-tail binding results in a "closed" conformation, with the C-terminal domain covering much of the surface of the FERM domain (32, 44). For ezrin, radixin and moesin, the CTD functions as a mask, blocking access of effector molecules, such as the cell surface receptors CD44 and ICAM2 and adaptor molecules, like EBP50/NHERF, to sites on the surface of the FERM domain (11, 25, 44). The interaction between the CTD and FERM domain is regulated by phosphatidyl inositol-(4,5)-bisphosphate (PIP_2) binding to the FERM domain and by phosphorylation of a critical residue in the CTD (3, 6, 10, 49). This residue, threonine 567 in ezrin, is conserved throughout the ERM family (21). Phosphorylation introduces a negative charge and a bulky side group that effectively reduces the affinity of the interaction, releasing the CTD from the FERM domain and causing a transition to an open conformation. Low-angle rotary shadowing electron microscopy (13) and biochemical studies (12) of purified radixin suggest that in the open conformation it is an extended filamentous structure with

* Corresponding author. Mailing address: Department of Cancer & Cell Biology, The Vontz Center for Molecular Studies, 3125 Eden Avenue, Cincinnati, OH 45267. Phone: (513) 558-3614. Fax: (513) 558-4454. E-mail: wallace.ip@uc.edu.

† Present address: Division of Experimental Hematology and Cancer Biology, Cincinnati Children's Hospital Medical Center, Cincinnati, OH 45229.

▽ Published ahead of print on 2 November 2009.

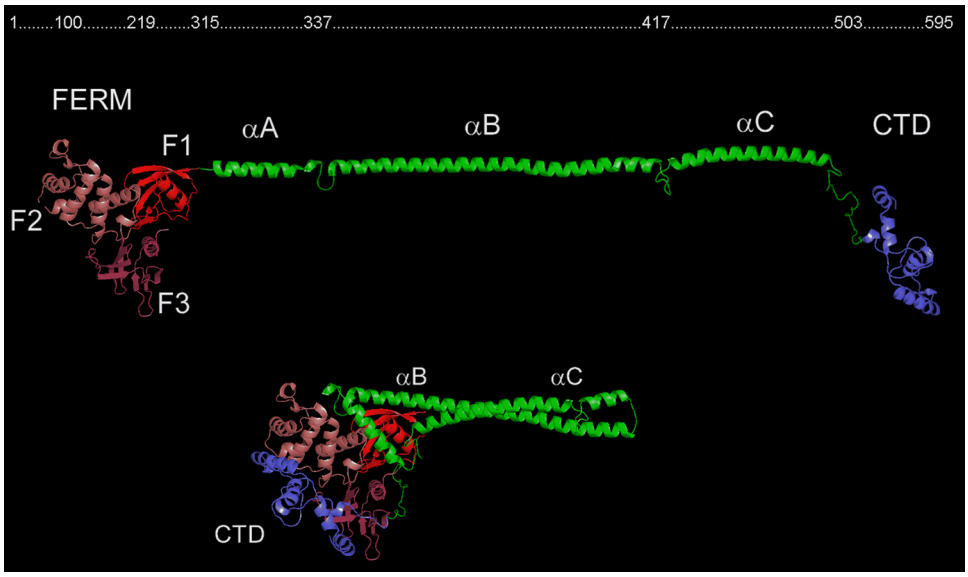

FIG. 1. ERM tertiary structure as represented by the crystal structure of full-length Sf-moesin (20), but with the merlin amino acid sequence substituted for Sf-moesin. Approximate boundary amino acid residues for all domains appear at the top of the figure. Each domain is assigned a different color. The ERM structure consists of an N-terminal FERM domain folded into three lobes, F1, F2, and F3. This is followed by a central α-helical domain containing three subhelices (αA, αB, and αC) and a CTD with four short helices. An ERM protein is thought to have an open conformation, an extended structure with the FERM domain and the CTD separated by the α-helical domain, that is more than 240 Å long. In the closed conformation, the α-helical domain bends at the αA-αB junction and again at the αB-αC junction, causing the CTD to be positioned over F2 and F3 of the FERM domain. More than half of the surface of the FERM domain is masked by interaction with the CTD, αA, and parts of αB and αC.

globular N and C termini that is greater than 240 Å in length. Signal transduction systems, such as the epidermal growth factor and Rho A pathways, induce phosphorylation of ERM proteins at the conserved C-terminal threonine via a number of kinases, including Rho kinase and protein kinase Cα (21, 28). Thus, conformational regulation of ERM proteins can be a point of integration of ERM activity with signal transduction pathways. The overall concept of ERM regulation, then, is centered upon a transition between an inactive, closed conformation that is mediated by the FERM-CTD interaction and an active, open conformation that is regulated by phosphorylation. In these two states, ERM proteins likely interact with different sets of binding partners, resulting in distinct functional outcomes.

Like the classical ERMs, merlin is also thought to be regulated by changes in conformation. The FERM domain and the CTD of merlin interact with each other, albeit at a lower level of affinity than the ezrin FERM domain and the CTD (29). There are important differences, however, between merlin and the other ERM proteins. First, phosphorylation of the conserved C-tail threonine T576 has not been reported to occur in mammalian merlin, and nonphosphorylatable and phosphomimetic substitutions at this site have no effect on merlin activity (42). Instead, merlin is phosphorylated at serine 518 in the CTD, a target of the p21-activated kinase PAK and protein kinase A (1, 18, 47). The growth-suppressive function of merlin is activated by dephosphorylation of S518 by the phosphatase PP1δ in a density-dependent manner (14). Second, it was reported in a study using FERM domain and CTD truncates of merlin that only cotransfection of both the N-and C-terminal halves resulted in growth suppression (38). Together, these observations suggested a model of inactive, phosphorylated merlin in an open conformation that, upon cell-to-cell contact, is dephosphorylated and transitions to a closed, growth suppressive conformation.

The existing model for conformational regulation described above is inferred from indirect data and assays that generally measure the interaction of isolated FERM and CTD truncates rather than full-length molecules (9, 29, 38). It has been impossible to test directly because tools have not been available to specifically assay for either the open or the closed form of merlin. Therefore, we have developed a series of probes that measures merlin conformation by fluorescence resonance energy transfer (FRET), both as purified protein and in live cells. Using these tools, we show that merlin exists predominately as a monomer in a stable, largely closed conformation. Additionally, we find that the closed conformation is largely mediated by the central α-helical domain; the contribution of the FERM-CTD interaction appears to be less significant than previously thought. Finally, we find that phosphorylation and protein interaction cause unexpectedly small changes in merlin conformation. We propose a new and more refined model for merlin regulation, in which merlin function is regulated by specific but subtle conformational changes that modulate the interaction between the FERM domain and the CTD.

MATERIALS AND METHODS

Cell culture. SC4 *Nf2*$^{-/-}$ Schwann cells were obtained from Marco Giovannini (House Ear Institute) and Helen Morrison (Leibniz Institute for Age Research). They were maintained in high-glucose-concentration Dulbecco's modified Eagle's medium (Mediatech) supplemented with 10% fetal bovine serum and penicillin streptomycin (Invitrogen) at 37°C, 10% CO_2, and 95% humidity. Cells

were transfected using Lipofectamine 2000 (Invitrogen) per the manufacturer's instructions.

Molecular biology. The merlin FRET probes were constructed from three founder plasmids, pCerulean-1 (David Piston, Vanderbilt University), pCMV-Venus (Dan Felsenfeld, Mt. Sinai School of Medicine), and pCMV-flag Merlin I. Cerulean is a green fluorescent protein (GFP) mutant with a blue-shifted emission spectrum that will act as a donor to Venus, a GFP mutant with a yellow-shifted emission spectrum (27, 34). DNA fragments were isolated from agarose gel and purified with a gel purification kit (Qiagen). Mini and maxi plasmid preparations were also performed with standard kits (Qiagen and Roche Applied Science). To generate the pC6V FRET control, Venus was cut from pCMV-Venus with BamHI and EcoRI and ligated into pCerulean-C1, which had been cut with BglII and EcoRI and dephosphorylated with shrimp alkaline phosphatase (SAP; Promega). To generate a second FRET control, pC23V the BamHI-EcoRI Venus fragment was cloned into BamHI-EcoRI-cut pCerulean-C1. To generate a vector that would easily accept merlin in frame to Cerulean and Venus, we generated an intermediate vector by placing a phosphorylated duplex adaptor oligonucleotide containing restriction sites for BspEI and SacI and overhanging cohesive ends for BspEI and BamHI. The sense strand is 5′-CCGGTCCGGACAGTGAGCTCG-3′. The antisense strand is 5′-GATCCG AGCTCACTGTCCGGA-3′. This adapter was cloned into BspEI-BamHI-cut pC23V. The resulting plasmid, designated pC-Ada-V, was found to have multiple copies of the adaptor primer, but the 5′ cloning BspEI site and the 3′ SacI site were in the correct frame relative to Cerulean and Venus to generate a fusion protein with a 35-amino-acid linker and to accept merlin. To generate pC-Mer-V, we cut merlin from pCMV-Flag-Merlin I with XmaI and SacI. XmaI and BspEI have compatible cohesive ends, and the SacI site in merlin straddles the penultimate amino acids. This fragment was cloned into the BspEI and SacI sites of SAP-treated pC-Ada-V to make pC-Mer-V. To clone C-Mer, the XbaI-EcoRI fragment from pCMV-flag-Merlin I, containing the merlin stop codon, was cloned into the BspEI and EcoRI sites of SAP-treated pC-Ada-V. To make pMer-V, the XmaI-SacI fragment of pCMV-flag Merlin I was cloned into pC-Ada-V, which had been cut with AgeI-SacI and treated with SAP. AgeI cuts pC-Ada-V upstream of Cerulean and generates compatible cohesive ends with BspEI, resulting in a fusion protein that initiates with the merlin start codon.

We generated deletions of the major domains by amplifying specific fragments of merlin, using pCMV-flag Merlin I as a template. The upstream PCR primers were designed with terminal XmaI and the downstream primers with a SacI site to fit into the BspEI and SacI sites of the pC-Ada-V vector. The FERM-Helix protein, from amino acid 1 to amino acid 502, was amplified using the upstream primer 5′-TGTCCCGGGAATGGCCGGAGCCATCGCTTCT-3′ and the downstream primer 5′-TGTGAGCTCACCAATGAGGTTGAAGC TTGG-3′. The Helix-CTD PCR product encompassing amino acids 315 to 595 was amplified using the upstream primer 5′-TGTGCTAGCATGTCTTT GGAAGTTCAGCAGATG-3′ and the downstream primer 5′-AAG TGG CAG GTC CTG GGG-3′. The Helix PCR product encompassing amino acids 315 to 502 was amplified using the upstream primer 5′-TGTCCCGGGATC TTTGGAAGTTCAGCAGTG-3′ and the downstream primer 5′-TGTGAG CTCACCAATGAGGTTGAAGCTTGG-3′. The FERM fragment from amino acid 1 to amino acid 314 was amplified using the upstream primer 5′-TGTCCCGGGAATGGCCGGAGCCATCGCTTCT-3′ and the downstream primer 5′-TGTGAGCTCATCGGCTTTCCTTCTCCTCAT-3′. PCR products were purified from an agarose gel, digested with XmaI and SacI, and then repurified from an agarose gel and ligated into BspE I-SacI cut, SAP-treated pC-Ada-V. All plasmids derived from PCR were fully sequenced on both strands to rule out PCR-induced mutation.

For bacterial expression and purification, we chose to first place a C-terminal epitope tag in Venus to facilitate future purification of full-length merlin. We generated a duplex adapter molecule that encoded an 8-amino-acid Strep tag, WSHPQFEK (52), followed by a stop codon, designed to be inserted in frame into the BsrGI site at the 3′ end of the Venus gene and the NotI site in the multiple-cloning site of pCMV-Venus. The sequences of this adapter are 5′-GTACAAGTGGAGCCACCCGCAGTTCGAAAAATAACG GCC-3′ (sense) and 5′-GGCCTTATTTTTCGAACTGCGGGTGGCTCCAC TT-3′ (antisense). The resulting plasmid is designated pCMV-VenusST. To move the Strep tag into pC-Mer-V, Venus was excised with BamHI and NotI and replaced with the compatible BamHI-EagI fragment from pCMV-VenusST to create pC-Mer-Vst. The C-Mer-Vst cassette was then excised with EcoRV and EagI and cloned into the EcoRV-NotI site of pET-30b(+). This plasmid, pET-C-Mer-Vst, expressed a protein with a His_6 tag N-terminal to Cerulean and the Strep tag C-terminal to Venus. The remaining bacterial expression clones, C6V, C-FERM-V, C-FERM-Helix-V, C-Helix-CTD-V, and C-Helix-V, were cloned by cutting with Eco47III and BsrGI and ligating into pET-C-Mer-Vst cut with EcoRV and BsrGI and treated with SAP. Unless otherwise noted, all biochemicals were purchased from Sigma and all restriction enzymes were from New England Biolabs. Custom oligonucleotides were purchased from Integrated DNA Technologies.

Protein purification. For purification, pET-30b(+)-based plasmids (Novagen) were transformed into the Rosetta2(DE3) *Escherichia coli* strain (Novagen), which is supplemented with tRNAs to match mammalian codon usage. Overnight cultures from a single colony were inoculated 1:20 in 500 ml of LB supplemented with kanamycin and chloramphenicol. The cultures were grown at 37°C with shaking at 200 rpm until an optical density at 600 nm of 0.8 to 1.2 was achieved and then cooled in an ice bath for 30 min. The culture was diluted 1:2 by adding 500 ml ice-cold LB containing 0.2 mM IPTG (isopropyl-β-D-thiogalactopyranoside) and 20 ml ethanol for final concentrations of 0.1 mM IPTG and 2% ethanol. To maximize expression of soluble protein, the culture was then incubated overnight at room temperature with shaking at 200 rpm. The cells were pelleted at 3,500 × *g* for 10 min at 4°C. The pellets were then weighed and snap frozen in liquid nitrogen. To harvest merlin protein, the pellets were thawed and resuspended in 5 ml per gram of lysis buffer (50 mM NaH_2PO_4, 300 mM NaCl, pH 7.5, 10 mM $MgCl_2$, 0.1% Triton X-100, 1 mM β-mercaptoethanol, 1:100 His_6 protease inhibitor cocktail [Sigma], 10 μg/ml DNase I, 100 μg/ml RNase I, 1 mg/ml lysozyme) and incubated at 4°C with agitation for 30 min. The lysate was then sonicated on ice for six cycles of 10 s on and 10 s off. Cell debris was pelleted at 14,000 × *g* for 30 min at 4°C, and the supernatant was saved.

Recombinant protein was recovered from lysate by dual affinity chromatography. Lysate was run over a nickel agarose column (Talon; Clontech); washed with 50 mM $NaHa_2PO_4$, 300 mM NaCl, pH 7.5, 20 mM imidazole; and then eluted in 50 mM NaH_2PO_4, 300 mM NaCl, pH 7.5, 1 mM β-mercaptoethanol, 250 mM imidazole. Eluted fractions were pooled and run over a streptactin column (IBA Biotagnology), washed with TBS (50 mM Tris-Cl, pH 7.5, 150 mM NaCl, 1 mM β-mercaptoethanol), and eluted with TBS-2.5 mM desthiobiotin (Sigma). Eluted fractions were pooled and analyzed for purity by Western blotting (see Fig. 4) and their protein concentrations determined by absorbance at 280 nm.

FRET spectrofluorometry. Spectrofluorometry was performed using a Horiba Jobin Yvon Fluorolog-3 spectrofluorometer. Purified proteins were analyzed at a concentration of 1 μM in TBS at room temperature. Samples were excited at 435 nm with a 5-nm slit width, and emission spectra were acquired from 450 nm to 600 nm at 1-nm intervals with a 2-nm slit width. Sodium dodecyl sulfate (SDS) was then added to each sample to give a 0.1% final concentration, and the emission spectra were measured again. SDS denatures the merlin structure without affecting the Cerulean or Venus fluorescence (2, 15), thus providing an internal negative control in each sample control for non-FRET-derived fluorescence. Transfected cell lysates were analyzed the same way, except using 5-nm slit widths at emission and excitation for enhanced sensitivity. The FRET signal (F) is expressed as a ratio of the acceptor emission (from 515 to 550 nm [$Em_{515\text{-}550}$]) to the donor emission (from 460 nm to 490 nm [$Em_{460\text{-}490}$]) with excitation at the donor's peak excitation wavelength of 435 nm (Ex_{435}): $F = Ex_{435}\ Em_{515\text{-}550}/Ex_{435}\ Em_{460\text{-}490}$. FRET efficiency ($E_{FRET}$) is expressed as normalized to the level for the SDS-denatured negative control: $E_{FRET} = 1 - (F_{SDS}/F_{FRET})$.

Analytical ultracentrifugation. Sedimentation velocity experiments were carried out at 20°C with a Beckman XL-I ProteomeLab analytical ultracentrifuge using absorbance optics. C-Mer-V and C-Helix-V proteins in 100 mM Tris, pH 7.5, 150 mM NaCl, 10 mM desthiobiotin, and 1 mM β-mercaptoethanol were loaded into two-sector charcoal-filled Epon centerpieces, spun at 36,000 rpm, and scanned at 280 nm. Data were analyzed using c(s) and c(M) models in the program Sedfit (36) to determine differential sedimentation coefficient (S) and apparent mass distributions, respectively.

Microscopy. SC4 cells were plated in 35-mm coverslip bottom dishes (Matek) and transfected as described above. After 24 h, cells were rinsed and the medium was replaced with phenol red-free Dulbecco's modified Eagle's medium containing 25 mM HEPES, pH 7.5. Cells were imaged live with a Zeiss Axioplan microscope using a 63× 1.4-numerical-aperture PlanApo water immersion objective, a Hammamatsu Orca ER camera, and a Uniblitz shutter controlled by Metamorph imaging software. The filter sets used for FRET were from Chroma. The excitation filter/dichroic mirror/emission filter sets for Cerulean were D436/20x, 455DCLP, and D480/40m; those for Venus were HQ515/20, Q515LP, and HQ535/30m; and those for FRET were D436/20x, 455DCLP, and HQ535/30m. The exposure times for donor, acceptor, and FRET channels were always held constant. Each field yielded three 1,280- by 1,024-pixel, 12-bit images, representing the donor, acceptor, and FRET channels. Ten fields were acquired for each transfection.

Image analysis. Images were analyzed using the Image J package (NIH). For the FRET/donor ratio images, the background was subtracted using a rolling-ball algorithm with a 50-pixel radius. A mask was then created by thresholding the

donor image and setting the background pixels to a value of 0 and the cell body pixels to a value of 1. The ratio image was generated by dividing the value for the background-subtracted FRET channel image by that for the background-subtracted donor channel image and multiplying the result by the value for the mask. The resulting 32-bit floating point image was used to measure the average pixel intensity in order to calculate FRET efficiencies. For display, 32-bit floating point images were converted to 8-bit images and then pseudocolored for intensity by using the Image J lookup table called Fire. The positive FRET control, C6V, and the negative FRET control, C-Mer, were used to set the upper and lower threshold scales for all ratio images. For display, the donor, acceptor, and FRET channel images were background subtracted as described above, converted into 8-bit images, and then pseudocolored using the cyan, yellow, and red lookup tables in Image J.

GST pulldowns. Glutathione *S*-transferase (GST)–NHERF was purchased from Addgene (plasmid 11636) (8). Expression in *E. coli* BL-21 was induced with IPTG. After lysis, GST or GST-NHERF was bound to glutathione beads and the beads were washed extensively. The amount of protein bound to the beads was determined by a Bradford assay (Bio-Rad). To assay for binding, an excess of GST or GST-NHERF beads was mixed with purified FRET probes and incubated at room temperature for 60 min with agitation in the dark. The beads were then transferred to disposable spin columns (Pierce) and centrifuged for 30 s at 3,000 × *g*, and the flowthrough was collected. The beads were washed four times with 500 μl TBS. GST proteins were eluted in four successive fractions with 100 mM glutathione in TBS, pH 7.5. For quantification, the fluorescence levels of aliquots of the input, flowthrough, wash, and eluate fractions were measured with a SpectraMax Gemini XPS plate fluorometer (Molecular Probes). The percent bound was calculated as the fluorescence in the pooled eluate fractions relative to the total fluorescence. The emission spectrum of the pooled eluate was measured as described above.

RESULTS

Merlin FRET probes. In crystal structures, the distance between the N- and C-terminal residues of ERM proteins in the closed conformation is 54 Å (Fig. 1) (20). When the molecule is in the open conformation, the length of merlin is predicted to be approximately 240 Å, suggesting that the open and closed conformations of merlin would be readily distinguishable by FRET, a sensitive technique that detects molecular interactions in the 10- to 100-Å range (40). To demonstrate this experimentally, we fused two GFP spectral variants, Cerulean and Venus, fused in frame to the N and C termini of merlin, to produce a FRET probe for merlin conformation, designated C-Mer-V (Fig. 2A). Additionally, to rule out the possibility of FRET signal emanating from antiparallel merlin dimers rather than from intramolecular FERM-CTD interaction, we constructed two more merlin fusion proteins: C-Mer, consisting of Cerulean fused in frame to the merlin N terminus, and Mer-V, consisting of Venus fused in frame to the merlin C terminus (Fig. 2A). We also constructed a positive control for FRET, C6V, consisting of Cerulean and Venus separated by a 6-amino-acid linker. Constructs were transfected into an immortalized Schwann cell line, SC4, derived from the conditional NF2$^{-/-}$ knockout mouse (7). Western blot analysis of transfected SC4 cell lysates showed that these constructs expressed stable fusion proteins of the appropriate size that react with both anti-merlin and anti-GFP antibodies (Fig. 2B).

C-Mer-V is biologically active. To determine if the addition of GFP variants to the N- and C-terminal ends of merlin interferes with function, we compared the abilities of the FRET probes to inhibit signal transduction cascades to untagged merlin, as measured by a transient AP-1 reporter assay (17). Cotransfection of C-Mer-V with an AP-1 reporter construct (−73 Col-Luc) significantly inhibited AP-1 activity relative to the level for a control transfection (Fig. 2C). Similarly,

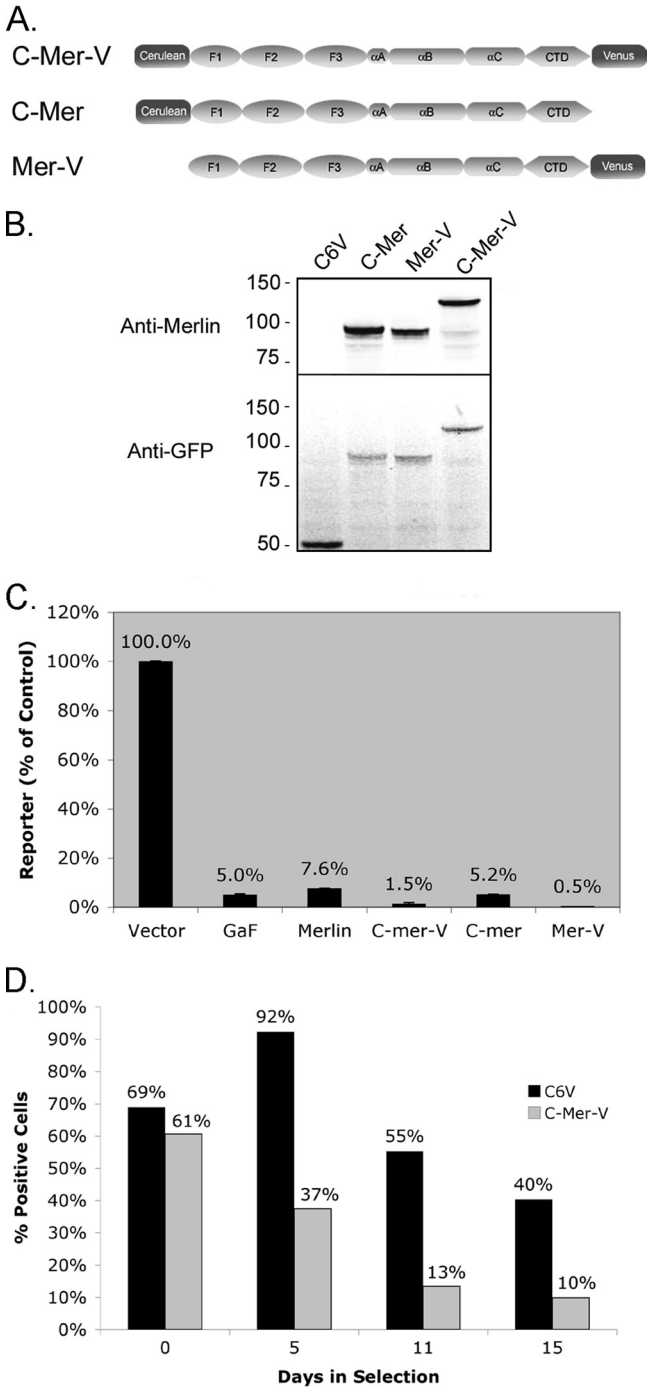

FIG. 2. Merlin FRET probes. (A) Schematic diagram of the intramolecular FRET probe C-Mer-V (top) and the intermolecular FRET probes C-Mer (middle) and Mer-V (bottom). (B) Immunoblot analysis of SC4 cell lysates transfected with the FRET positive control C6V, C-Mer, Mer-V, or C-Mer-V, probed with antibodies to merlin (upper panel) or GFP (lower panel). Molecular mass markers in kDa are on the left. (C) AP-1 reporter gene assays of SC4 cells cotransfected with the reporter −73-Col-Luc and the indicated plasmid. Luciferase assays were normalized to merlin expression levels. (D) SC4 cells transfected with either C6V or C-Mer-V, and the proportion of positive cells were counted by flow cytometry after incubation in G418 for the indicated number of days.

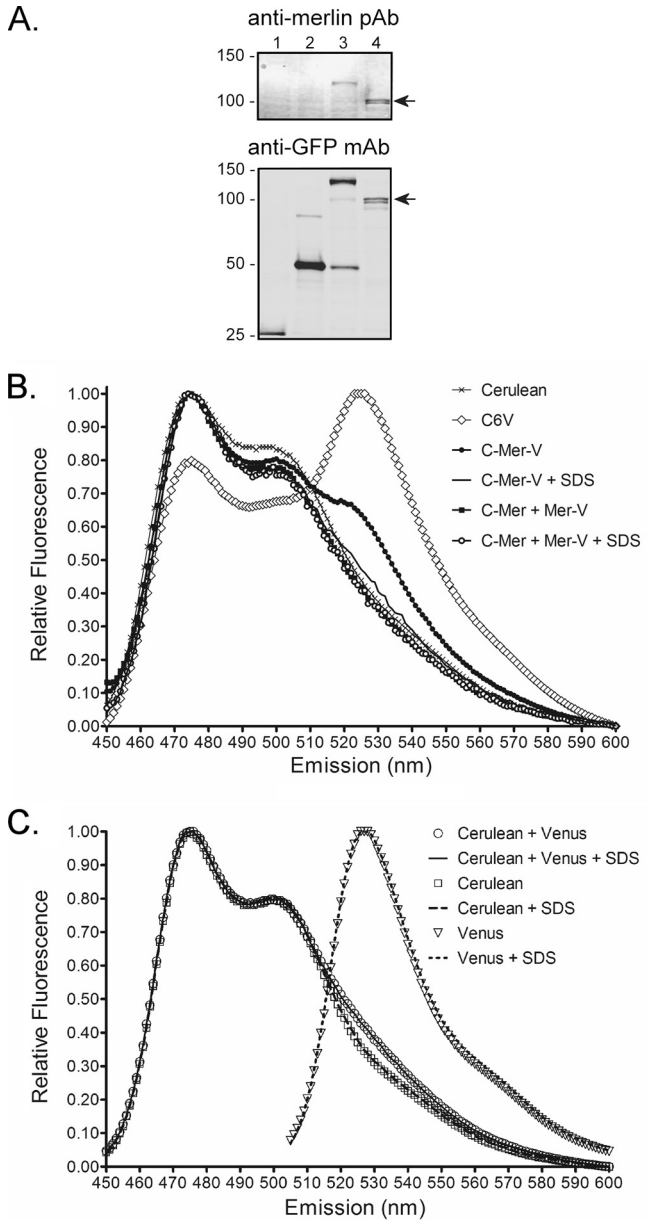

FIG. 3. Merlin FRET in cell lysates. (A) Immunoblot analysis of SC4 cells transfected with Cerulean (lane 1), C6V (lane 2), C-Mer-V (lane 3), and C-Mer and Mer-V (lane 4). The doublets of both Western blots in lane 4 (arrows) indicate equal expression of C-Mer and Mer-V. The lower blot for C-Mer-V shows significant low-molecular-mass contaminants that were recognized by the anti-GFP antibody, suggesting proteolysis. The presence of these contaminants, which could lead to overestimation of FRET, prompted us to use dual tag affinity purified bacterially expressed proteins for further studies. Molecular mass markers in kDa are on the left. (B) Emission spectra of lysates from transfected SC4 cells, excited at 435 nm and measured at room temperature. For this and all subsequent figures, all raw fluorescence values are normalized to the maximum value obtained in a given scan such that all plotted values are ≤ 1. This allows all spectra in a given experiment to be presented in a single graph, regardless of the differences in the expression levels of the constructs used. The fluorescence of C-Mer-V between 515 nm and 550 nm is FRET that arises due to the proximity of the two fluorophores. FRET does not occur in a cotransfection of C-Mer and Mer-V, ruling out dimerization as the cause of FRET. Addition of 0.1% SDS to C-Mer-V abolishes the FRET, indicating that FRET requires properly folded merlin. The scans for C-Mer/Mer-V in the presence and absence of SDS are essentially superimposable and therefore difficult to discern. (C) Emission spectra showing that fluorescence of Cerulean and Venus is not affected by the addition of 0.1% SDS. Lysates from Cerulean-transfected and Cerulean-Venus-cotransfected cells were excited at 435 nm. Lysate from Venus-transfected cells was excited at 490 nm.

the single-fusion proteins C-Mer and Mer-V also significantly inhibited AP-1 activity (Fig. 2C). This effect was on par with inhibition by untagged merlin and a dominant-negative AP-1 control construct, GFP-A-fos (GaF) (Fig. 2C), and suggests that the fusion of fluorescent proteins to either end of C-Mer-V does not destroy the merlin function. To assess the effect of C-Mer-V on growth, we performed a flow cytometry-based clonogenic assay on SC4 cells. The outgrowth of C-Mer-V-positive G418-resistant cells was reduced compared to the level for a C6V control (Fig. 2D), indicating that growth inhibition was not affected by the fusion of Cerulean and Venus to either terminus of merlin. These experiments argue against any dramatic abrogation of merlin function in the FRET probes; however, subtle differences in merlin activity caused by the presence of the N- and C-terminal GFP molecules cannot be ruled out.

Merlin FRET derives from monomers. To further validate the FRET probes as tools for measurement of merlin conformation, we performed spectrofluorometry on cell lysates derived from transfected SC4 cells. Western blot analysis of the lysates verified that C-Mer and Mer-V were expressed to equimolar levels (Fig. 3A). FRET is measured as the fluorescence intensity at the acceptor's peak emission wavelength (515 nm to 550 nm) relative to the intensity at the donor peak emission wavelength (460 nm to 490 nm) with excitation at the donor's peak excitation wavelength (435 nm). As a positive FRET control, SC4 cells were transfected with the C6V plasmid, and cells transfected with Cerulean alone were used as a reference spectrum. Lysate from untransfected cells was used to subtract signal resulting from possible autofluorescence in the cell lysates. As a negative control for FRET, we treated the cell lysates with 0.1% SDS, which denatures merlin but does not affect the fluorescent proteins to which it is fused (2, 15) (Fig. 3C). This treatment provided a negative control that has the same molar ratio of Cerulean to Venus as the untreated fusion protein. The emission spectrum of C-Mer-V-transfected cell lysates had a clear FRET signal in the 515- to 550-nm range. SDS treatment resulted in a complete loss of FRET signal, indicating that the FRET required properly folded merlin (Fig. 3B). The detection of a measurable FRET signal in transfected mammalian cell lysate suggests a population of C-Mer-V that exists in a closed conformation. In contrast, the emission spectrum of the cell lysate derived from the C-Mer/Mer-V cotransfection had no FRET signal, and addition of SDS did not change the spectrum (Fig. 3B), suggesting that the FRET detected with C-Mer-V is due to interaction between Cerulean and Venus within the same molecule. This experiment demonstrates the feasibility of the FRET strategy and suggests that merlin exists as a monomer in a closed conformation.

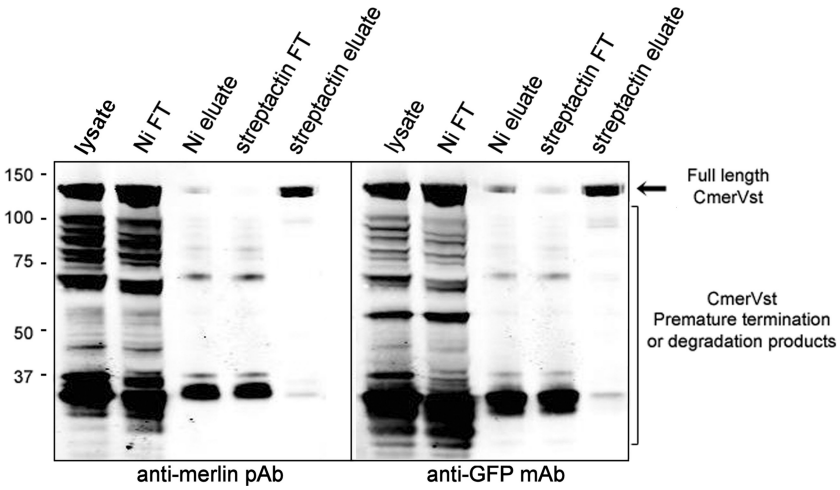

FIG. 4. Purification of C-Mer-V from bacterial cell lysates. Results are shown for immunoblot analysis of aliquots sampled during purification of C-Mer-V from bacterial cell lysates, probed with antibodies to merlin (left) and GFP (right). Ni FT, nickel column flowthrough; Ni eluate, eluate from the nickel column; streptactin FT, streptactin column flowthrough; streptactin eluate, eluate from the streptactin column.

Ablation of the FERM-CTD interaction is insufficient to generate the open conformation. The preliminary experiments using transfected cell lysates serve as a proof of principle for the FRET study. To make more-accurate measurements under better-defined conditions, we purified merlin FRET fusion proteins from a bacterial expression system by using a dual affinity tag protocol (Fig. 4). The use of tags at both ends of merlin ensured that the expressed product was full-length and that the two fluorophores, Cerulean and Venus, would be present at equimolar amounts during FRET measurement. Additionally, to identify the merlin sequences responsible for this closed conformation, we constructed variants of C-Mer-V with deletions in its major domains (Fig. 5A). We constructed a deletion mutant of the CTD, C-FERM-Helix-V, that is unable to engage in the FERM-CTD interaction. According to current views, this variant would be predicted to exist in a constitutively open conformation. The converse construct, C-Helix-CTD-V, lacks the FERM domain and would also be expected to be in a constitutively open conformation. An additional construct, C-Helix-V, consisted of the central helix region alone, devoid of both the FERM domain and the CTD. Finally, the C-FERM-V construct contains the FERM domain alone. SDS-polyacrylamide gel electrophoresis and infrared protein staining demonstrate that full-length C-Mer-V and mutant proteins were purified to near-homogeneity from the bacterial expression system (Fig. 5B).

The FRET efficiency of purified, full-length C-Mer-V was measured at a concentration of 1 μM, in 150 mM NaCl, pH 7.5, at room temperature. As was done with cell lysates, samples were treated with 0.1% SDS to denature merlin and to establish a baseline emission spectrum from which we calculated the FRET efficiency. Measurements using trypsin-digested C-Mer-V as the negative baseline produced essentially identical FRET efficiencies (data not shown). Additionally, the FRET measurements were performed with 2.5 M NaCl to further rule out FRET resulting from dimerization, since purified preparations of merlin exist primarily as monomers at high salt concentrations (29).

Under these conditions, purified C-Mer-V had a FRET efficiency of 0.311, consistent with measurements obtained from mammalian cell lysates (Fig. 5B). Although the distance between the two fluorophores could not be calculated exactly, because of the lack of information on κ^2, the angle between the fluorophore dipoles within C-Mer-V (33), this FRET efficiency indicates that C-Mer-V is not in an open conformation in which the merlin moiety is in an unfurled configuration ~240 Å in length but exists in a folded conformation similar to that described to occur in the moesin crystal structure (20). FRET from C-Mer-V was completely abolished in 0.1% SDS, indicating that merlin secondary structure is required for effective FRET (Fig. 5C). The FRET efficiency of C-Mer-V was dramatically increased in 2.5 M NaCl (Fig. 5C), suggesting that merlin conformation is sensitive to local ionic conditions and ruling out dimerization as a source of the FRET signal. In contrast, the FRET signal from C6V was only minimally affected by high salt concentration and reduced in 0.1% SDS (Fig. 5H), most likely due to a relaxation of the unstructured amino acids linking Cerulean and Venus in this protein.

Of considerable surprise, the FRET efficiency of C-FERM-Helix-V, which lacked the CTD, was also high, at 0.303 (Fig. 5D), and showed an additional increase in 2.5 M NaCl. These values are very similar to those obtained from full-length C-Mer-V and strongly suggest that even in the absence of a FERM-CTD interaction merlin nevertheless exhibits FRET, most probably because it exists in a closed conformation. This notion is further supported by results from the FERM deletion mutant C-Helix-CTD-V, which also had a FRET efficiency of 0.343 and a hypertonic contraction (Fig. 5E). Likewise, the helix domain alone, encoded by the C-Helix-V construct, had a FRET efficiency of 0.346 and contracted under hypertonic conditions (Fig. 5F). On the basis of our finding that mutants lacking the FERM domain, the CTD, or both all had significant levels of intramolecular FRET, we conclude that ablating the FERM-CTD interaction is insufficient to force merlin into a constitutively open conformation but that the central α-helical domain alone is sufficient to cause merlin to assume the closed conformation.

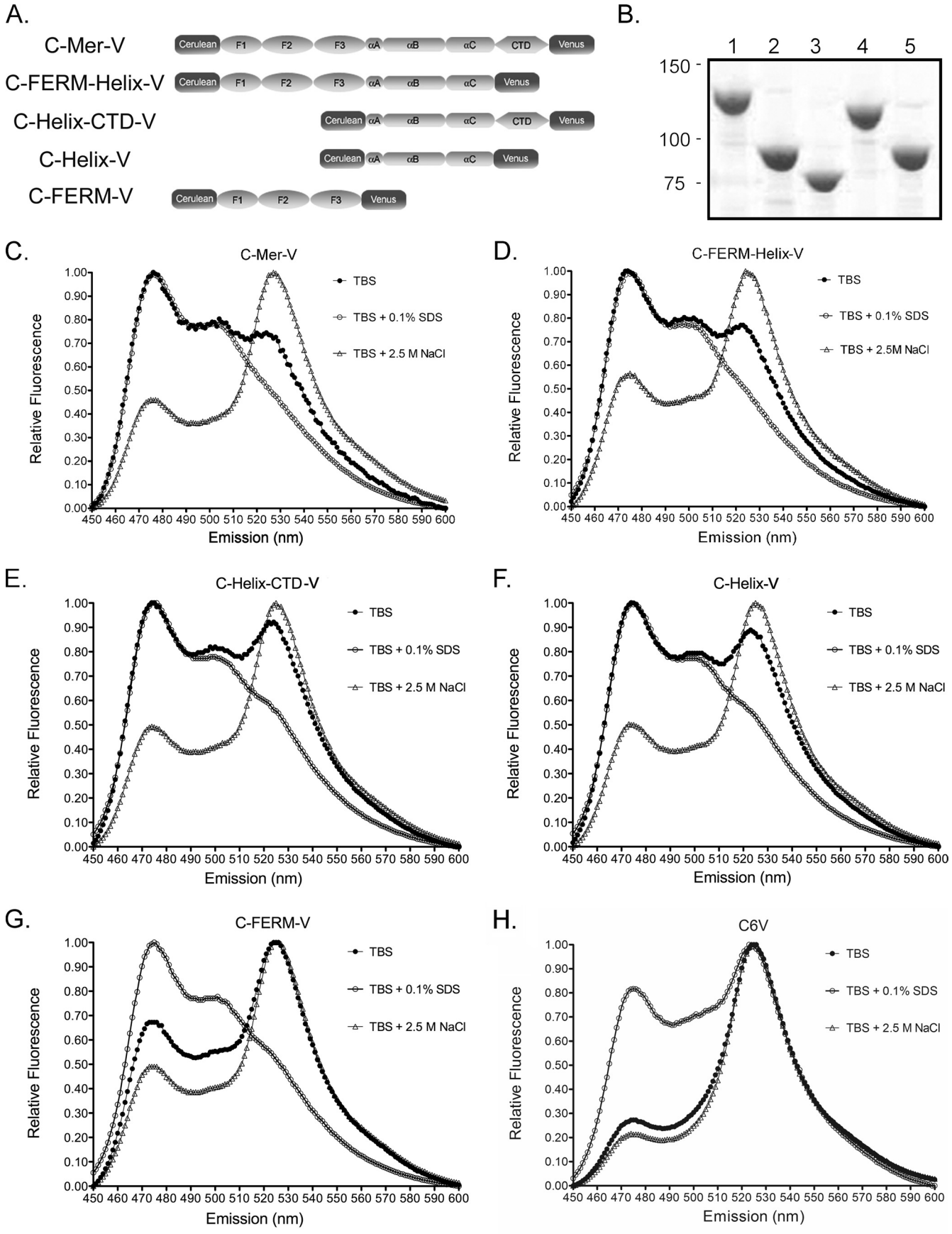

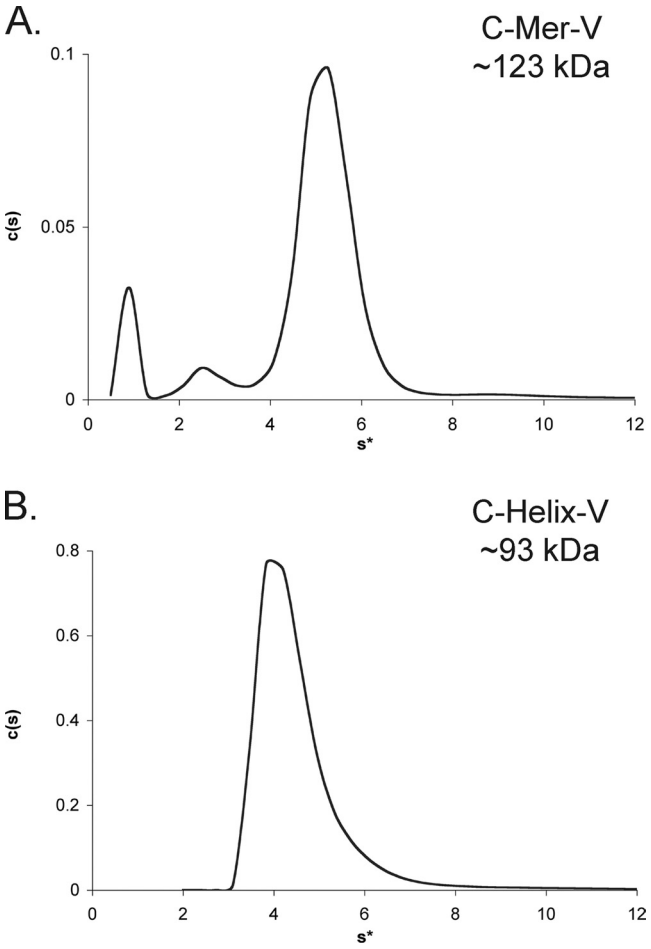

FIG. 6. Analytical ultracentrifugation studies of purified C-Mer-V and C-Helix-V. (A) The *S* distribution of C-Mer-V, as measured by absorbance at 280 nm, yielded an *S* value of 5.3 ± 0.65, with an apparent molecular mass of ~123 kDa and an f/f_0 value of 1.693. (B) The *S* distribution of C-Helix-V yielded an *S* value of 4.5 ± 0.80, with an apparent molecular mass of ~95.4 kDa and an f/f_0 value of 1.679.

Interestingly, the C-FERM-V construct, which encodes only the FERM domain, displayed a very strong FRET signal, with an efficiency of 0.595 (Fig. 5G). Treatment with 0.1% SDS completely abolished its FRET signal, while 2.5 M NaCl slightly increased the FRET efficiency, possibly resulting from contraction of the domain.

Analytical ultracentrifugation. Measured spectroscopically, a FRET signal is an average of the behavior of all molecules present in solution. This may result from a single population of molecules in a given conformation or from a mixture of open and closed conformations. To distinguish between these possibilities, we performed sedimentation velocity experiments with an analytical ultracentrifuge to directly measure the shapes, sizes, and hydrodynamic parameters of the C-Mer-V and C-Helix-V proteins. Our data indicate that C-Mer-V sediments predominantly as a single population of monomers, with an *S* value of 5.3 ± 0.65 and an apparent molecular mass of ~123 kDa (Fig. 6A), in close agreement with its calculated molecular mass of 130 kDa. The frictional coefficient (f/f_0) is 1.693, consistent with an elongated molecule with a prolate axial ratio of 9.35. C-Helix-V also sedimented as a monomer, with an *S* value of 4.5 ± 0.80 and an apparent molecular mass of ~95.4 kDa (Fig. 6B). This is again in close agreement with the predicted molecular mass of 96.6 kDa. The f/f_0 value for C-Helix-V is 1.679, also consistent with an elongated molecule with a prolate axial ratio of 9.15. The analytical ultracentrifugation experiments were carried out under the same conditions as those used to measure FRET, and their results unambiguously rule out the contribution of dimeric or multimeric complexes to FRET in the purified C-Mer-V and C-Helix-V preparations. Just as important, the similar prolate axial ratios of C-Mer-V and C-Helix-V again support the notion that the closed conformation of the central α-helix is maintained in the absence of the two end domains.

Merlin conformation in live cells. Results from cotransfection of C-Mer and Mer-V, FRET signal in the deletion mutants, and the analytical ultracentrifuigation experiments demonstrate that merlin exists primarily as a folded monomer in vitro. We sought to test this in vivo, in the context of living cells, by performing FRET imaging on SC4 Schwann cells that expressed our merlin constructs. Live, unfixed cells expressing each of the merlin deletion mutants were imaged using filter sets for the donor, acceptor, and FRET channels. The ratio of the emission in FRET channel to that in the donor channel, the FRET/donor ratio, is an indication of the level of FRET, and to display the FRET signals optimally, we generated pseudocolor images based on this ratio. In cells transfected with the C6V positive-control plasmid, the FRET/donor ratio was high, confirming a high level of FRET. In contrast, a negative control consisting of cells expressing C-Mer showed a low FRET/donor ratio. We used these two FRET/donor ratios to set the upper and lower thresholds of the pseudocolor display.

In transfected SC4 cells, C-Mer-V was localized to the cell periphery and dynamic actin structures (Fig. 7), as expected (48). The ratio image shows a clearly detectable level of FRET. The ratio images are also homogeneous, supporting our in vitro experiments showing that the merlin population exists as a single conformation. The C-FERM-Helix-V protein, which lacked the CTD, also displayed a marked localization to the cell periphery, identical to that seen with full-length C-Mer-V (Fig. 7). The FRET/donor ratio of C-FERM-Helix-V was similar to that of the full-length protein and in line with the FRET efficiency measured by spectrofluorometry. The FERM deletion mutant C-Helix-CTD-V had a strikingly different distri-

FIG. 5. Deletion mutants of merlin for FRET studies. (A) Schematic diagram of the deletion mutants that removed the CTD (C-FERM-Helix-V), the FERM domain (C-Helix-CTD-V), both the FERM domain and the CTD (C-Helix-V), or both Helix and the CTD (C-FERM-V). (B) Infrared protein stain of 5-μg aliquots of purified bacterially expressed proteins. Lanes: 1, C-Mer-V; 2, C-FERM-V; 3, C-Helix-V; 4, C-FERM-Helix-V; 5, C-Helix-CTD-V. (C to H) Emission spectra from 450 nm to 600 nm, excited at 435 nm. Results are shown for 1 μM purified proteins at 20°C in TBS, TBS with 0.1% SDS, and 2.5 M NaCl.

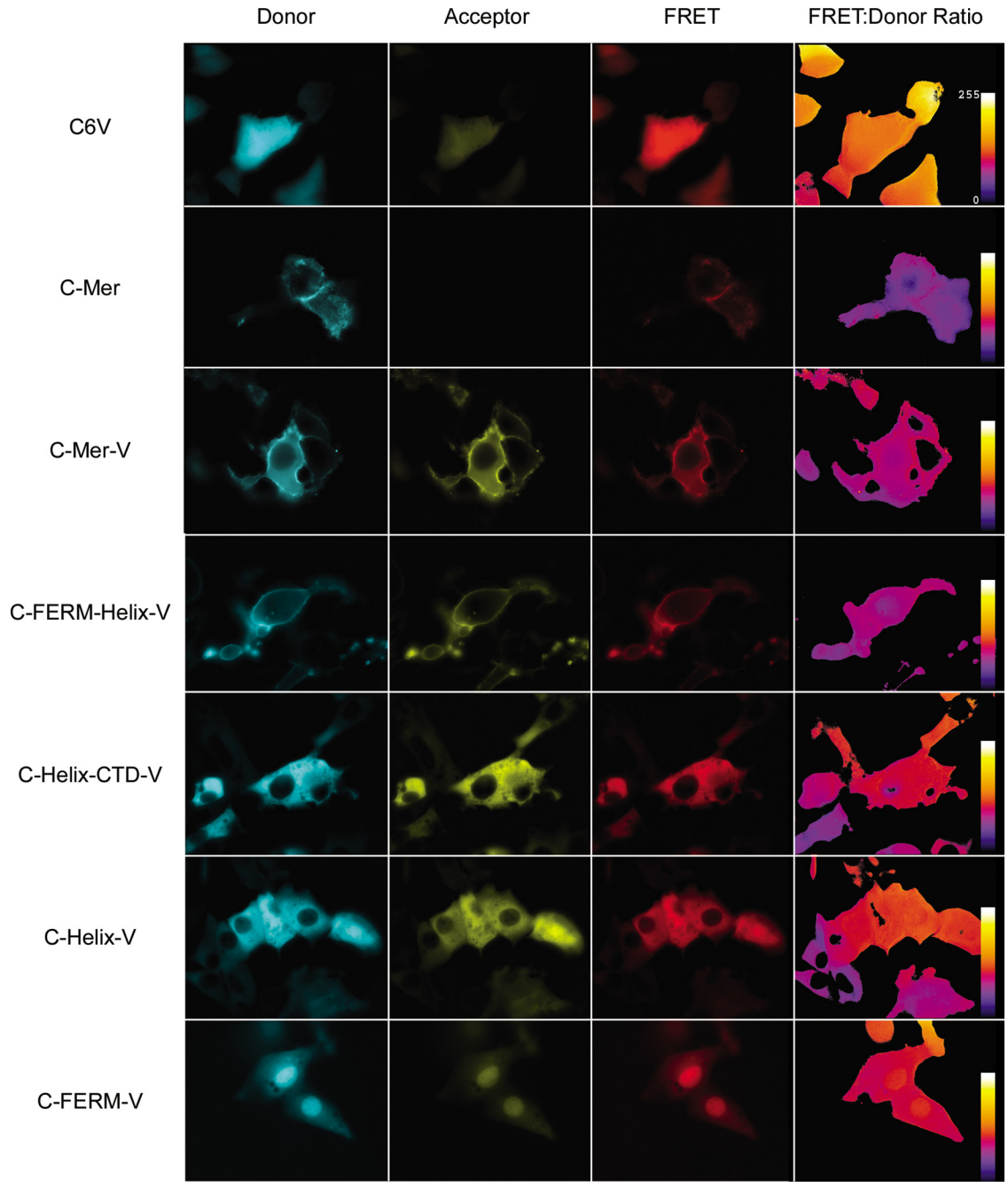

FIG. 7. C-Mer-V in live cells. SC4 cells were transfected with the indicated plasmids. Images were acquired using specific filter sets for the donor, acceptor, and FRET signals. The FRET efficiency is represented by the ratio of the FRET channel to the donor channel. The images were pseudocolored using the FRET ratios of the C6V positive control and the C-Mer negative control to set the upper and lower thresholds.

bution, localizing to the cytoplasm with a higher FRET/donor ratio, again reflecting the spectrofluorometric data. The localization and FRET/donor ratio of the C-Helix-V protein were identical to those of C-Helix-CTD-V. The construct expressing the FERM domain alone, C-FERM-V, had a higher FRET/donor ratio, consistent with the in vitro data. Interestingly, C-FERM-V was predominately localized to the nucleus. The full implication of this is unclear at this point, but at 90 kDa, C-FERM-V is too large to passively diffuse into the nucleus, suggesting active transport. In general, FRET/donor ratios derived from multiple images representing living cells are remarkably consistent and in close agreement with the spectroscopic data obtained from the corresponding purified proteins, indicating that these ratios accurately represent the conformation of the deletion mutants in vivo and supporting the idea that merlin exists in a constitutively closed conformation.

Effect of phosphorylation on merlin conformation. Phosphorylation at serine 518 is believed to inactivate merlin by converting

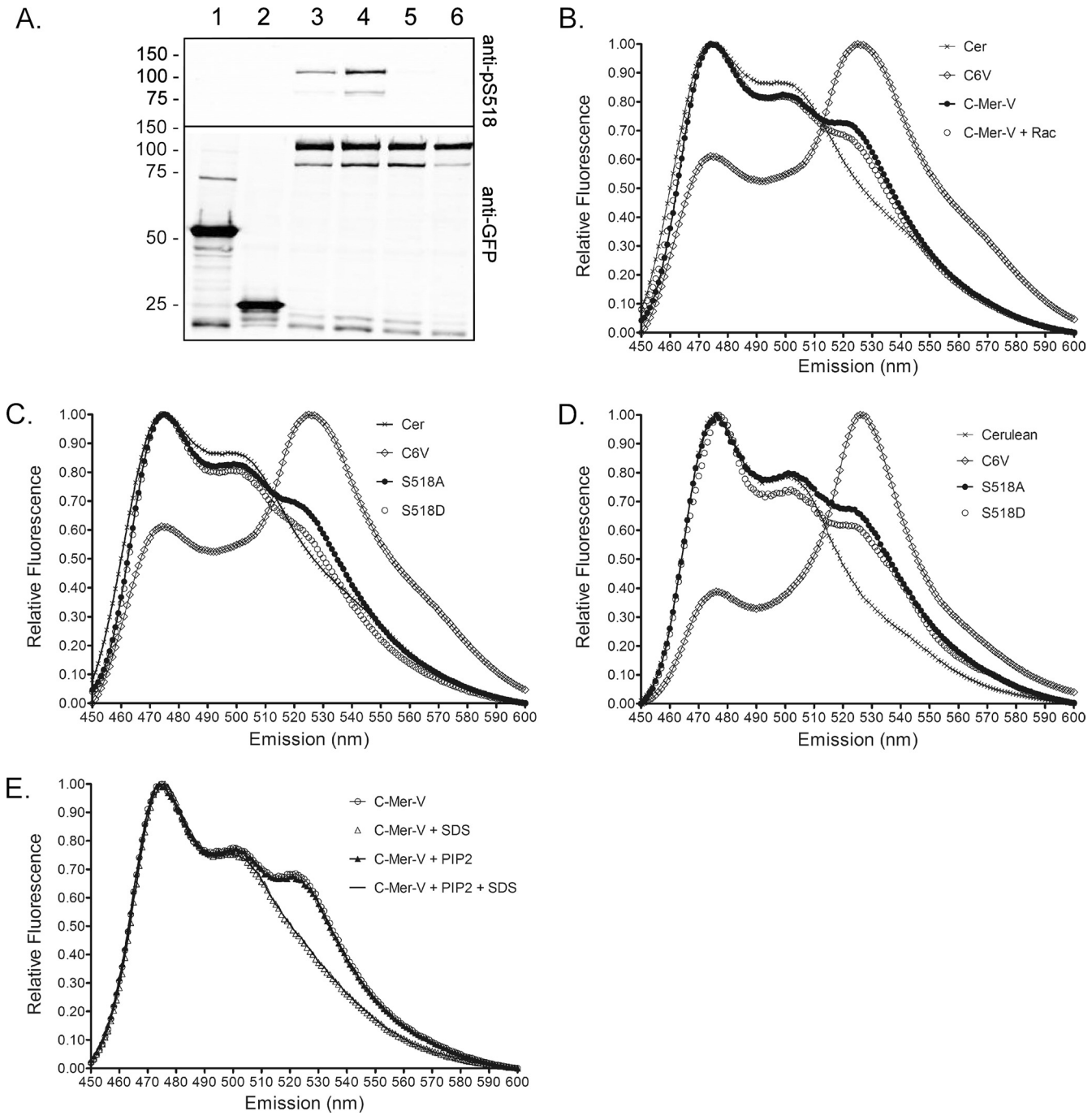

FIG. 8. Effect of phosphorylation on merlin conformation. (A) Immunoblot analysis of lysates from transfected SC4 cells. The blots are probed with anti-phospho-S518 merlin (upper panel) and anti-GFP antibodies (lower panel). Lanes: 1, C6V; 2, Cerulean; 3, C-Mer-V/empty vector cotransfection; 4, C-Mer-V/Rac cotransfection; 5, C-Mer^{S518A}-V; 6, C-Mer^{S518D}-V. Molecular mass in kDa is indicated on the left. (B) Effect of Rac-induced hyperphosphorylation of merlin. Results are shown for emission spectra of lysates from transfected SC4 cells, excited at 435 nm and measured at room temperature. (C) Emission spectra of lysates of SC4 cells expressing S518 nonphosphorylatable and phosphomimetic mutants of merlin, excited at 435 nm and measured at room temperature. (D) Emission spectra of 1 μM purified C-Mer^{S518A}-V and C-Mer^{S518D}-V at 20°C in TBS, excited at 435 nm. (E) Effect of PIP_2 on C-Mer-V conformation. Shown are emission spectra of 1 μM purified proteins at 20°C in TBS, excited at 435 nm, for C-Mer-V, C-Mer-V with 0.1% SDS, C-Mer-V with 10 μM PIP_2, and C-Mer-V with 10 μM PIP_2 with 0.1% SDS.

it into an open conformation (35). To determine if this conformational change is detectable by FRET, we cotransfected SC4 cells with C-Mer-V and activated Rac, which induces phosphorylation of merlin at S518 via the effector kinase PAK (37). Spectrofluorometry carried out on lysates of cotransfected cells showed a very modest decrease in FRET efficiency relative to lysates with C-Mer-V and an empty vector (Fig. 8B), despite a significant increase in phosphorylation at S518 (Fig. 8A).

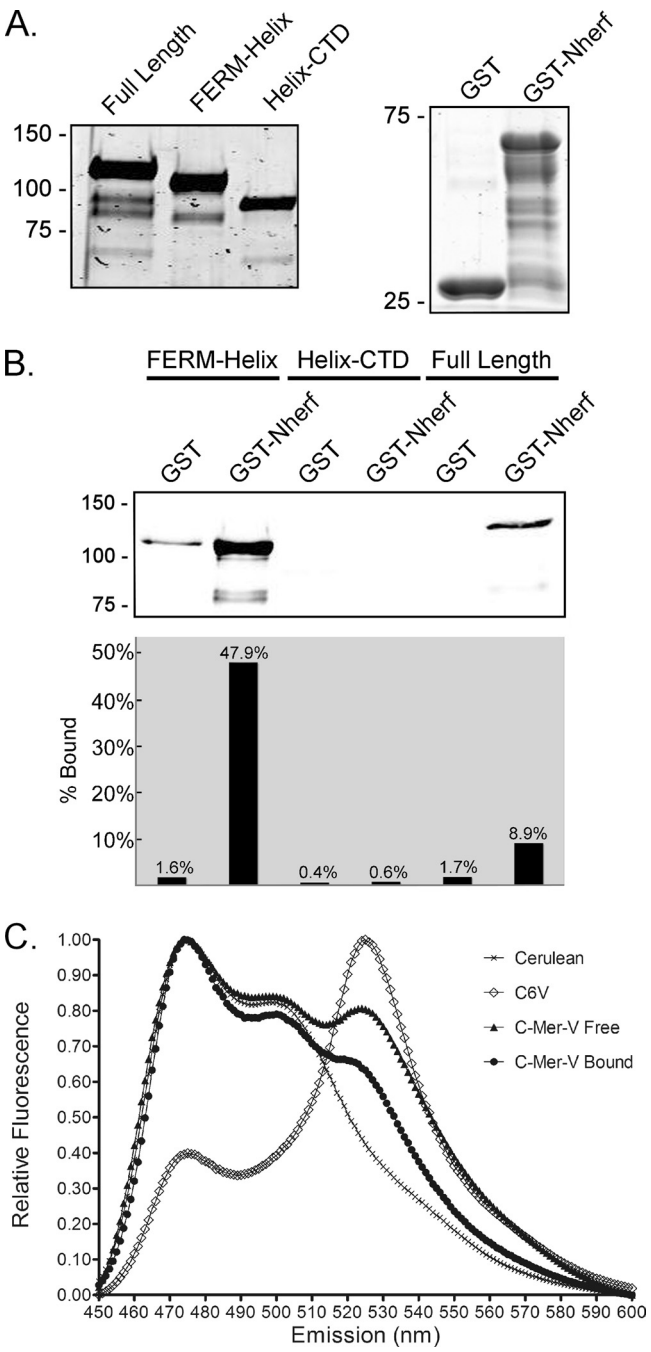

FIG. 9. Conformation of merlin bound to GST-NHERF. (A) Input prey proteins, from left to right: C-Mer-V, C-FERM-Helix-V, and C-Helix-CTD-V, followed by the bait proteins GST and GST-NHERF. (B) (Upper panel) Immunoblot analysis of eluates from the GST pulldown experiments probed with anti-GFP antibodies. Left to right: C-FERM-Helix-V/GST, C-FERM-Helix-V/GST-NHERF, C-Helix-CTD-V/GST, C-Helix-CTD-V/GST-NHERF, C-Mer-V/GST, C-Mer-V/GST-NHERF. (Lower panel) Quantification of GST pulldowns by fluorescence measurements of the pooled eluates. (C) Emission spectra of GST-NHERF-bound C-Mer-V and unbound C-Mer-V with the Cerulean negative control and the C6V positive control. Binding of GST-NHERF to merlin causes a slight loss in FRET, indicating a subtle change toward the open state but not a full unfurling of the α-helical domain as was suggested previously.

This result suggests that phosphorylation at S518 does not dramatically influence merlin conformation. An alternative interpretation, however, is that only a subpopulation of merlin molecules was phosphorylated or that the merlin molecules in the cell were phosphorylated to various degrees. In this scenario, the modest FRET signal that we obtained would be an average for all merlin molecules in a spectrum of conformation. To resolve this question, we examined the FRET behavior of two mutant C-Mer-V variants with a phosphomimetic aspartic acid substitution (S518D) and a nonphosphorylatable alanine substitution (S518A). Surace et al. (42) reported previously that, in biological assays, these mutant merlin species behave as fully phosphorylated and fully dephosphorylated merlin. Both mutants showed small differences in FRET efficiency in purified, bacterially expressed proteins and in transfected mammalian cell lysates (Fig. 8C and D).

In ezrin, binding to PIP_2 is believed to precede phosphorylation of T567, a triggering event for opening of the molecule (3, 6, 10, 49), and we and others have observed that merlin binds PIP_2 (30) (T. Mani, J.-J. Meng, and W. Ip, unpublished). We therefore examined if the presence of PIP_2 would have an effect on the conformation of merlin. As shown in Fig. 8E, the FRET efficiency of C-Mer-V is essentially unchanged by the addition of PIP_2 in vitro.

Taken together, these experiments show that while S518 phosphorylation has detectable effects on merlin conformation, as revealed by FRET measurements, the effects are subtle, far less than might have been expected on the basis of the current model.

Conformation of the merlin-NHERF complex. The merlin binding protein, EBP50/NHERF, binds to the same groove in the FERM domain as does the CTD domain (43). Therefore, in the C-Mer-V–NHERF complex, where the CTD is displaced by NHERF, merlin exists in what is by definition an "open" conformation. Measuring FRET in C-Mer-V when it is in complex with NHERF, therefore, will determine the magnitude of the shift from the closed to the open conformation.

We used GST pulldown to isolate full-length C-Mer-V bound to GST-NHERF. As a positive control, we also isolated the C-FERM-Helix-V mutant, which lacks the CTD and is expected to bind GST-NHERF efficiently. As a negative control, we used C-Helix-CTD-V, the mutant that lacks the FERM domain, the site of NHERF binding (Fig. 9A). The FRET probes were mixed with either GST-NHERF beads or GST beads in excess and repeatedly washed to remove merlin not bound to NHERF. The bound merlin was then eluted with glutathione. Any merlin that is present in the eluate is thus fully bound to NHERF and in the open state. Binding was quantified by measuring the fluorescence of the proteins bound to GST-NHERF.

As expected, the merlin FERM-Helix specifically bound GST-NHERF but not GST. Conversely, Helix-CTD did not bind GST-NHERF. Full-length C-Mer-V also specifically bound to GST-NHERF, but much less efficiently than C-FERM-Helix-V (Fig. 9B). FRET analysis of the fraction of C-Mer-V that was GST-NHERF bound, and therefore fully open, showed that when in a complex with GST-NHERF, C-Mer-V has a slightly lower FRET efficiency than unbound material, suggesting a conformational shift toward the open state (Fig. 9C). This result provides independent confirmation

that the transition between the active and inactive states of merlin involves a subtle conformational shift rather than a full unfurling into an extended form.

DISCUSSION

The data presented here confirm that changes in merlin activity are accompanied by changes in conformation but suggest that the mechanism and magnitude of these changes differ substantially from those predicted by the current model. Our studies employed FRET, utilizing two variants of GFP, Cerulean and Venus, as the donor and acceptor pair, fused in frame to the N and C termini of merlin, respectively. Since the efficiency of energy transfer is inversely proportional to the sixth power of the distance between the donor and acceptor, FRET is a sensitive spectroscopic and microscopic technique for measuring molecular proximity in the 10- to 100-Å range (33). Initially, the FRET-based strategy was judged to be feasible on the basis of two crystal structures for the closely related ERM protein moesin. In both structures, consisting of the moesin FERM complexed with the CTD (32) and a 3-Å resolution structure of full-length Sf-moesin (20), the distance between the N- and the C-terminal amino acids is 54 Å, well within the practical range of FRET for Cerulean and Venus. Furthermore, FRET has been successfully used for both radixin (12) and ezrin (50, 51).

We validated our FRET probes by demonstrating that they were functionally equivalent to untagged merlin by two criteria: inhibition of signal transduction and growth suppression. C-Mer-V inhibited the activity of the oncogene-induced immediate-early transcription factor AP-1 as effectively as untagged merlin. C-Mer-V also curtailed SC4 cell viability in a clonogenic assay. It remains possible that the function of C-Mer-V is different from that of untagged merlin in subtle ways that we have not tested, but at the level of our analysis, the addition of reporter proteins to either end of merlin did not abrogate its activity.

We detected FRET in C-Mer-V by spectrofluorometry in both transfected SC4 cell lysates and purified, bacterially expressed preparations. The efficiency of the FRET signal in these experiments was on par with the published values for radixin and ezrin (12, 50, 51). We excluded the possibility that FRET signal could result from the dimerization of donor- and acceptor-labeled merlin in three ways. First, coexpression of C-Mer and Mer-V in cells at equivalent levels did not produce FRET, ruling out merlin dimerization in a head-to-tail or antiparallel fashion. Second, we observed FRET in a high-salt environment, a condition known to favor merlin in the monomeric form (29). Finally, analytical ultracentrifugation experiments demonstrated unequivocally that purified C-Mer-V exists predominately as a monomer, with essentially no dimeric or oligomeric species. These data argue strongly that, in both purified protein preparations and mammalian cell lysates, the FRET arose from a population of merlin monomers in the closed conformation.

We then used FERM domain and CTD deletion mutants to identify merlin sequences responsible for the closed conformation. If the FERM-CTD interaction is responsible for the closed conformation, as favored by the current model, then the deletions should cause the molecule to unfold into an open conformation, resulting in a loss of the FRET signal. Surprisingly, all four deletion mutants displayed FRET efficiencies equivalent to or greater than that of the full-length C-Mer-V protein, as measured by both spectroscopy and live cell microscopy. In particular, C-Helix-V, the mutant that lacked both the FERM domain and the CTD, had a robust FRET signal that increased in a high-salt environment. As demonstrated by analytical ultracentrifugation, it is monomeric and has a prolate axial ratio very similar to that of the full-length molecule, C-Mer-V. As FRET emanating from a monomeric population of molecules can be explained only by the helix folding over on itself, and this folding occurs even in the absence of the FERM domain and the CTD, these results imply that the central helical domain plays a role in specifying this closed conformation and, at the same time, suggest that the role of the FERM-CTD interaction may be less essential than previously thought.

Measurement of C-Mer-V FRET under conditions of well-defined merlin activity showed that merlin does not undergo large-scale structural changes as it becomes activated or inactivated. Hyperphosphorylation of S518, brought about by expression of activated Rac, inactivates merlin and "opens" the molecule (37). In lysates derived from cells overexpressing activated Rac, we observed only a very small decrease in C-Mer-V FRET efficiency. To ensure that the FRET change was not due to a shift in the proportions of phosphorylated and unphosphorylated merlin, we measured FRET of merlin with the phosphomimetic and nonphosphorylatable substitutions at S518, S518D and S518A, and found that these also had modest effect on FRET in purified proteins and in mammalian cell lysates. It is important to note, however, that the small difference in FRET efficiency between phosphorylated and unphosphorylated merlin is real and reproducible and suggests that C-Mer-V is indeed slightly more closed in its unphosphorylatable state in spite of the subtlety of the conformational changes.

FRET measurement of merlin isolated in an obligatory open state further supports the hypothesis that merlin undergoes structural changes of limited range. This was achieved by GST pulldown using the FERM domain binding partner, NHERF. FRET analysis reveals that C-Mer-V bound to GST-NHERF is slightly more open than unbound merlin but that the fluorophores are nevertheless still close enough to support FRET, consistent with the small shift in conformation seen in the phosphorylation experiments.

Finally, FRET microscopy of live cells revealed that the FRET/donor ratio of C-Mer-V is relatively constant across the cell, with little or no variance of signal from different subcellular structures. The subcellular uniformity in FRET efficiency suggests that merlin conformation is relatively homogeneous within the cell.

To summarize, by analyzing purified merlin and cell lysates containing merlin of known phosphorylation states, by measuring the FRET efficiency of fully ligand-bound merlin, and by analyzing merlin FRET efficiency in live cells, we found no evidence that inactive merlin unfolds into an extended conformation that separates the FERM domain and the CTD by more than 100 Å, thereby putting them out of FRET range. Therefore, the transition between the inactive and active states does not involve large-scale folding and unfolding of merlin as previously believed.

While our results differ from the generally accepted model of ERM conformational regulation, they are consistent with the only published X-ray crystal structure of a full-length ERM protein, Sf-moesin (20). This structure depicts the central α-helical domain as consisting of three subhelices, αA, αB, and αC, whose critical feature is that αC folds back on αB to form an antiparallel coiled coil that juxtaposes the CTD and the FERM domain. The coiled-coil nature of the central α-helical domain may explain the behavior of C-Mer-V at different salt concentrations. The strength of a coiled coil is dependent upon interactions between the side chains of hydrophobic amino acids at the "a" and "d" positions of the heptad repeat. Salt concentrations greater than 1 M have the general effect of strengthening the hydrophobic interactions within and between proteins and can screen unfavorable electrostatic interactions (5). Thus, at 2.5 M NaCl, the coiled coil formed by the αB and αC helices may tighten, bringing the N and C termini closer together, resulting in increased FRET efficiency. This observation highlights the possibility that the central α-helix may be an important point of control for ERM function, as has been suggested by Li et al. in their study of Sf-moesin (20). One could envision the central α-helical region as the site of posttranslational modification or of protein interaction that changes the mean distance between the FERM domain and the CTD, thereby controlling the access of effector proteins to the FERM domain. This may be a more energetically feasible way to control access to the FERM domain than to completely unfold the central α-helical domain, a highly stable coiled coil for the most part. This is also consistent with the modest changes in conformation seen under different S518 phosphorylation states and in the GST pulldown experiments. Clearly, the function of the CTD is to block access of effector proteins, like NHERF, to the FERM domain, but this may be achieved by subtle differences in the FERM-CTD interaction rather than dramatic changes in overall structure.

There is evidence that other ERM proteins may exist in extended, open conformations. Analytical ultracentrifugation and electron microscopy studies of purified radixin suggest that it can exist as an asymmetric, 249-Å by 19-Å rod (12). This may be explained by differences between the merlin and ERM primary structures. The radixin central helix, like those of ezrin and moesin, has a large number of polar amino acids that may form ionic interactions and surface salt bridges that stabilize an extended helix (12, 41). The merlin central α-helical region has far fewer acidic and basic amino acids, possibly favoring the stability of the coiled coil over the extended form (12, 19).

Our results paint a picture of merlin conformational regulation that is more subtle and complex than was previously envisioned. It seems likely that the regulation of merlin is not a binary, on/off switch between active and inactive states. It is also likely that merlin conformation is not defined by either a fully open molecule with unfettered access to the FERM domain or a completely closed molecule with no access. Instead, we propose that the FERM domain and the CTD are maintained in close proximity at all times by the central α-helical region, which is folded into a hairpin shape that is stabilized by an antiparallel coiled-coil structure. Subtle changes in the FERM-CTD interaction may be regulated by mechanisms that act on the central α-helical coiled-coil, resulting in small alterations in the distance between the FERM domain and the CTD, thereby regulating the affinity of this interaction and modulating how it masks binding sites for effector proteins on the FERM domain surface. The critical point of merlin regulation, then, is the cooperation between the FERM-CTD interaction and the central α-helical region to provide more-fine-tuned and nuanced access to docking sites on the FERM domain, which implies a more sophisticated regulation of merlin tumor suppressor function.

ACKNOWLEDGMENTS

We are grateful to Robert Brackenbury, Shyra Miller, and Brad Ozanne for critical reading of the manuscript and Dan Felsenfeld and David Piston for the kind gift of the Venus and Cerulean plasmids. We also thank Chia-chi Ho and Peixuan Guo for the use of their equipment.

This work was supported by awards R01-CA78524 from the National Cancer Institute and NF043043 from the Department of Defense CDMRP Neurofibromatosis Research Program to W.I. A.B.H. is supported by funds from the Ohio Eminent Scholar program. T.M. is the recipient of a Young Investigator Award from the Children's Tumor Foundation.

REFERENCES

1. **Alfthan, K., L. Heiska, M. Gronholm, G. H. Renkema, and O. Carpen.** 2004. Cyclic AMP-dependent protein kinase phosphorylates merlin at serine 518 independently of p21-activated kinase and promotes merlin-ezrin heterodimerization. J. Biol. Chem. **279:**18559–18566.
2. **Alkaabi, K. M., A. Yafea, and S. S. Ashraf.** 2005. Effect of pH on thermal- and chemical-induced denaturation of GFP. Appl. Biochem. Biotechnol. **126:**149–156.
3. **Barret, C., C. Roy, P. Montcourrier, P. Mangeat, and V. Niggli.** 2000. Mutagenesis of the phosphatidylinositol 4,5-bisphosphate (PIP(2)) binding site in the NH(2)-terminal domain of ezrin correlates with its altered cellular distribution. J. Cell Biol. **151:**1067–1080.
4. **Bretscher, A., D. Chambers, R. Nguyen, and D. Reczek.** 2000. ERM-Merlin and EBP50 protein families in plasma membrane organization and function. Annu. Rev. Cell Dev. Biol. **16:**113–143.
5. **Burkhard, P., S. Ivaninskii, and A. Lustig.** 2002. Improving coiled-coil stability by optimizing ionic interactions. J. Mol. Biol. **318:**901–910.
6. **Fievet, B. T., A. Gautreau, C. Roy, L. Del Maestro, P. Mangeat, D. Louvard, and M. Arpin.** 2004. Phosphoinositide binding and phosphorylation act sequentially in the activation mechanism of ezrin. J. Cell Biol. **164:**653–659.
7. **Giovannini, M., E. Robanus-Maandag, M. van der Valk, M. Niwa-Kawakita, V. Abramowski, L. Goutebroze, J. M. Woodruff, A. Berns, and G. Thomas.** 2000. Conditional biallelic Nf2 mutation in the mouse promotes manifestations of human neurofibromatosis type 2. Genes Dev. **14:**1617–1630.
8. **Gonzalez-Agosti, C., T. Wiederhold, M. E. Herndon, J. Gusella, and V. Ramesh.** 1999. Interdomain interaction of merlin isoforms and its influence on intermolecular binding to NHE-RF. J. Biol. Chem. **274:**34438–34442.
9. **Gronholm, M., M. Sainio, F. Zhao, L. Heiska, A. Vaheri, and O. Carpen.** 1999. Homotypic and heterotypic interaction of the neurofibromatosis 2 tumor suppressor protein merlin and the ERM protein ezrin. J. Cell Sci. **112**(6)**:**895–904.
10. **Hamada, K., T. Shimizu, T. Matsui, S. Tsukita, and T. Hakoshima.** 2000. Structural basis of the membrane-targeting and unmasking mechanisms of the radixin FERM domain. EMBO J. **19:**4449–4462.
11. **Hamada, K., T. Shimizu, S. Yonemura, S. Tsukita, S. Tsukita, and T. Hakoshima.** 2003. Structural basis of adhesion-molecule recognition by ERM proteins revealed by the crystal structure of the radixin-ICAM-2 complex. EMBO J. **22:**502–514.
12. **Hoeflich, K. P., S. Tsukita, L. Hicks, C. M. Kay, S. Tsukita, and M. Ikura.** 2003. Insights into a single rod-like helix in activated radixin required for membrane-cytoskeletal cross-linking. Biochemistry **42:**11634–11641.
13. **Ishikawa, H., A. Tamura, T. Matsui, H. Sasaki, T. Hakoshima, S. Tsukita, and S. Tsukita.** 2001. Structural conversion between open and closed forms of radixin: low-angle shadowing electron microscopy. J. Mol. Biol. **310:**973–978.
14. **Jin, H., T. Sperka, P. Herrlich, and H. Morrison.** 2006. Tumorigenic transformation by CPI-17 through inhibition of a merlin phosphatase. Nature **442:**576–579.
15. **Kain, S. R., and P. Kitts.** 1997. Expression and detection of green fluorescent protein (GFP). Methods Mol. Biol. **63:**305–324.
16. **Kang, B. S., D. R. Cooper, Y. Devedjiev, U. Derewenda, and Z. S. Derewenda.** 2002. The structure of the FERM domain of merlin, the neurofibromatosis type 2 gene product. Acta Crystallogr. D Biol. Crystallogr. **58:**381–391.
17. **Kim, H., J. Y. Lim, Y. H. Kim, H. Kim, S. H. Park, K. H. Lee, H. Han, S. S.**

Jeun, J. H. Lee, and H. K. Rha. 2002. Inhibition of ras-mediated activator protein 1 activity and cell growth by merlin. Mol. Cells **14:**108–114.
18. **Kissil, J. L., K. C. Johnson, M. S. Eckman, and T. Jacks.** 2002. Merlin phosphorylation by p21-activated kinase 2 and effects of phosphorylation on merlin localization. J. Biol. Chem. **277:**10394–10399.
19. **Kohn, W. D., C. M. Kay, and R. S. Hodges.** 1997. Salt effects on protein stability: two-stranded alpha-helical coiled-coils containing inter- or intra-helical ion pairs. J. Mol. Biol. **267:**1039–1052.
20. **Li, Q., M. R. Nance, R. Kulikauskas, K. Nyberg, R. Fehon, P. A. Karplus, A. Bretscher, and J. J. Tesmer.** 2007. Self-masking in an intact ERM-merlin protein: an active role for the central alpha-helical domain. J. Mol. Biol. **365:**1446–1459.
21. **Matsui, T., M. Maeda, Y. Doi, S. Yonemura, M. Amano, K. Kaibuchi, S. Tsukita, and S. Tsukita.** 1998. Rho-kinase phosphorylates COOH-terminal threonines of ezrin/radixin/moesin (ERM) proteins and regulates their head-to-tail association. J. Cell Biol. **140:**647–657.
22. **McClatchey, A. I.** 2003. Merlin and ERM proteins: unappreciated roles in cancer development? Nat. Rev. Cancer **3:**877–883.
23. **McClatchey, A. I., I. Saotome, K. Mercer, D. Crowley, J. F. Gusella, R. T. Bronson, and T. Jacks.** 1998. Mice heterozygous for a mutation at the Nf2 tumor suppressor locus develop a range of highly metastatic tumors. Genes Dev. **12:**1121–1133.
24. **McClatchey, A. I., I. Saotome, V. Ramesh, J. F. Gusella, and T. Jacks.** 1997. The Nf2 tumor suppressor gene product is essential for extraembryonic development immediately prior to gastrulation. Genes Dev. **11:**1253–1265.
25. **Mori, T., K. Kitano, S. Terawaki, R. Maesaki, Y. Fukami, and T. Hakoshima.** 2008. Structural basis for CD44 recognition by ERM proteins. J. Biol. Chem. **283:**29602–29612.
26. **Morrison, H., L. S. Sherman, J. Legg, F. Banine, C. Isacke, C. A. Haipek, D. H. Gutmann, H. Ponta, and P. Herrlich.** 2001. The NF2 tumor suppressor gene product, merlin, mediates contact inhibition of growth through interactions with CD44. Genes Dev. **15:**968–980.
27. **Nagai, T., K. Ibata, E. S. Park, M. Kubota, K. Mikoshiba, and A. Miyawaki.** 2002. A variant of yellow fluorescent protein with fast and efficient maturation for cell-biological applications. Nat. Biotechnol. **20:**87–90.
28. **Ng, T., M. Parsons, W. E. Hughes, J. Monypenny, D. Zicha, A. Gautreau, M. Arpin, S. Gschmeissner, P. J. Verveer, P. I. Bastiaens, and P. J. Parker.** 2001. Ezrin is a downstream effector of trafficking PKC-integrin complexes involved in the control of cell motility. EMBO J. **20:**2723–2741.
29. **Nguyen, R., D. Reczek, and A. Bretscher.** 2001. Hierarchy of merlin and ezrin N- and C-terminal domain interactions in homo- and heterotypic associations and their relationship to binding of scaffolding proteins EBP50 and E3KARP. J. Biol. Chem. **276:**7621–7629.
30. **Okada, M., Y. Wang, S. W. Jang, X. Tang, L. M. Neri, and K. Ye.** 2009. Akt phosphorylation of merlin enhances its binding to phosphatidylinositols and inhibits the tumor-suppressive activities of merlin. Cancer Res. **69:**4043–4051.
31. **Okada, T., M. Lopez-Lago, and F. G. Giancotti.** 2005. Merlin/NF-2 mediates contact inhibition of growth by suppressing recruitment of Rac to the plasma membrane. J. Cell Biol. **171:**361–371.
32. **Pearson, M. A., D. Reczek, A. Bretscher, and P. A. Karplus.** 2000. Structure of the ERM protein moesin reveals the FERM domain fold masked by an extended actin binding tail domain. Cell **101:**259–270.
33. **Piston, D. W., and G. J. Kremers.** 2007. Fluorescent protein FRET: the good, the bad and the ugly. Trends Biochem. Sci. **32:**407–414.
34. **Rizzo, M. A., G. H. Springer, B. Granada, and D. W. Piston.** 2004. An improved cyan fluorescent protein variant useful for FRET. Nat. Biotechnol. **22:**445–449.
35. **Rong, R., E. I. Surace, C. A. Haipek, D. H. Gutmann, and K. Ye.** 2004. Serine 518 phosphorylation modulates merlin intramolecular association and binding to critical effectors important for NF2 growth suppression. Oncogene **23:**8447–8454.
36. **Schuck, P.** 2000. Size-distribution analysis of macromolecules by sedimentation velocity ultracentrifugation and lamm equation modeling. Biophys. J. **78:**1606–1619.
37. **Shaw, R. J., J. G. Paez, M. Curto, A. Yaktine, W. M. Pruitt, I. Saotome, J. P. O'Bryan, V. Gupta, N. Ratner, C. J. Der, T. Jacks, and A. I. McClatchey.** 2001. The Nf2 tumor suppressor, merlin, functions in Rac-dependent signaling. Dev. Cell **1:**63–72.
38. **Sherman, L., H. M. Xu, R. T. Geist, S. Saporito-Irwin, N. Howells, H. Ponta, P. Herrlich, and D. H. Gutmann.** 1997. Interdomain binding mediates tumor growth suppression by the NF2 gene product. Oncogene **15:**2505–2509.
39. **Shimizu, T., A. Seto, N. Maita, K. Hamada, S. Tsukita, S. Tsukita, and T. Hakoshima.** 2002. Structural basis for neurofibromatosis type 2. Crystal structure of the merlin FERM domain. J. Biol. Chem. **277:**10332–10336.
40. **Shimozono, S., and A. Miyawaki.** 2008. Engineering FRET constructs using CFP and YFP. Methods Cell Biol. **85:**381–393.
41. **Smith, J. S., and J. M. Scholtz.** 1998. Energetics of polar side-chain interactions in helical peptides: salt effects on ion pairs and hydrogen bonds. Biochemistry **37:**33–40.
42. **Surace, E. I., C. A. Haipek, and D. H. Gutmann.** 2004. Effect of merlin phosphorylation on neurofibromatosis 2 (NF2) gene function. Oncogene **23:**580–587.
43. **Terawaki, S., R. Maesaki, and T. Hakoshima.** 2006. Structural basis for NHERF recognition by ERM proteins. Structure **14:**777–789.
44. **Terawaki, S., R. Maesaki, K. Okada, and T. Hakoshima.** 2003. Crystallographic characterization of the radixin FERM domain bound to the C-terminal region of the human Na+/H+-exchanger regulatory factor (NHERF). Acta Crystallogr. D Biol. Crystallogr. **59:**177–179.
45. **Trofatter, J. A., M. M. MacCollin, J. L. Rutter, J. R. Murrell, M. P. Duyao, D. M. Parry, R. Eldridge, N. Kley, A. G. Menon, K. Pulaski, et al.** 1993. A novel moesin-, ezrin-, radixin-like gene is a candidate for the neurofibromatosis 2 tumor suppressor. Cell **72:**791–800.
46. **Turunen, O., M. Sainio, J. Jaaskelainen, O. Carpen, and A. Vaheri.** 1998. Structure-function relationships in the ezrin family and the effect of tumor-associated point mutations in neurofibromatosis 2 protein. Biochim. Biophys. Acta **1387:**1–16.
47. **Xiao, G. H., A. Beeser, J. Chernoff, and J. R. Testa.** 2002. p21-activated kinase links Rac/Cdc42 signaling to merlin. J. Biol. Chem. **277:**883–886.
48. **Xu, H. M., and D. H. Gutmann.** 1998. Merlin differentially associates with the microtubule and actin cytoskeleton. J. Neurosci. Res. **51:**403–415.
49. **Yonemura, S., T. Matsui, S. Tsukita, and S. Tsukita.** 2002. Rho-dependent and -independent activation mechanisms of ezrin/radixin/moesin proteins: an essential role for polyphosphoinositides in vivo. J. Cell Sci. **115:**2569–2580.
50. **Zhu, L., Y. Liu, and J. G. Forte.** 2005. Ezrin oligomers are the membrane-bound dormant form in gastric parietal cells. Am. J. Physiol. Cell Physiol. **288:**C1242–1254.
51. **Zhu, L., R. Zhou, S. Mettler, T. Wu, A. Abbas, J. Delaney, and J. G. Forte.** 2007. High turnover of ezrin T567 phosphorylation: conformation, activity, and cellular function. Am. J. Physiol. Cell Physiol. **293:**C874–C884.
52. **Zwicker, N., K. Adelhelm, R. Thiericke, S. Grabley, and F. Hanel.** 1999. Strep-tag II for one-step affinity purification of active bHLHzip domain of human c-Myc. BioTechniques **27:**368–375.